Abass, Adeyinka; Wada, Kentaro; Matsunaga, Hisao; Remes, Heikki; Vuorio, Tiina

Quantitative Characterization of the Spatial Distribution of Corrosion Pits Based on Nearest Neighbor Analysis

Published in:
Corrosion

DOI:
10.5006/3551

Published: 01/09/2020

Document Version
Peer-reviewed accepted author manuscript, also known as Final accepted manuscript or Post-print

Published under the following license:
Unspecified

Please cite the original version:
Abass, A., Wada, K., Matsunaga, H., Remes, H., & Vuorio, T. (2020). Quantitative Characterization of the Spatial Distribution of Corrosion Pits Based on Nearest Neighbor Analysis. *Corrosion*, *76*(9), 861-870. https://doi.org/10.5006/3551

Quantitative Characterization of the Spatial Distribution of Corrosion-Pits based on Nearest-Neighbour Analysis

Adeyinka Abass[a, b *], Kentaro Wada[a, c], Hisao Matsunaga[c, d, e, f], Heikki Remes[g], Tiina Vuorio[h]

[a] Graduate School of Engineering, Kyushu University, 744 Moto-oka, Nishi-ku, Fukuoka 819-0395, Japan

[b] Konecranes Global Corporation, Koneenkatu 8, Hyvinkää, FI-05801, Finland

[c] AIST–Kyushu University Hydrogen Materials Laboratory (HydoMate), National Institute of Advanced Industrial Science and Technology (AIST), 744 Moto-oka, Nishi-ku, Fukuoka 819-0395, Japan

[d] Department of Mechanical Engineering, Kyushu University, 744 Moto-oka, Nishi-ku, Fukuoka 819-0395, Japan

[e] Research Center for Hydrogen Industrial Use and Storage (HYDROGENIUS), Kyushu University, 744 Moto-oka, Nishi-ku, Fukuoka 819-0395, Japan

[f] International Institute for Carbon-Neutral Energy Research (WPI-I2CNER), Kyushu University, 744 Moto-oka, Nishi-ku, Fukuoka 819-0395, Japan

[g] Aalto University, School of Engineering, Department of Mechanical Engineering, PO BOX 13400, FI-00076, Finland

[h] Häme University of Applied Science, HAMK Tech Research Unit, Visakaarre 9, FI-13100, Finland

*Corresponding author:

abass.adeyinka.073@s.kyushu-u.ac.jp
744 Moto-oka, Nishi-ku, Fukuoka 819-0395, Japan

Author contributions

Adeyinka Abass: Conceptualization, Software, Formal analysis, Investigation, Writing - original draft

Kentaro Wada: Resources, Project administration, Writing - review and editing

Hisao Matsunaga: Supervision, Funding acquisition, Writing - review and editing

Heikki Remes: Writing - review and editing

Tiina Vuorio: Resources, Writing - review and editing

Abstract

Nearest-Neighbour Analysis (NNA)-based procedures are proposed for the quantitative characterization of the spatial distribution of corrosion pits in metals. After the exposure of a carbon steel to a 3.5%-NaCl-solution mist, the results derived from observation of corrosion-pit initiation and growth were used to justify the applicability of this approach. The pits initially comprised clusters that were superimposed on a randomly distributed background set. The clustered pits subsequently coalesced, evolving into a more random pit-arrangement. Furthermore, it was revealed that in the early stages, the spatial pit-distribution can be predicted via inspection of surface inclusions prior to the corrosion process.

Keywords

Steel; Statistics; Corrosion fatigue; Inclusion; Pitting corrosion; Environmental effects

1. Introduction

The detrimental effect caused by the combination of cyclic-loading and a corrosive environment has been acknowledged from as early as the beginning of the 19th century [1]. Although there remains some disagreement amongst researchers about the corrosion-fatigue, fracture-process details, there exists a consensus about the critical role of corrosion-pits in the initiation of fatigue-cracks [1-7].

Numerous fracture mechanics-based models have been proposed for assessing the corrosion fatigue-life of structures and machinery, particularly those destined to be subjected to cyclic-loading in corrosive environments. Such techniques have commonly focused on the individual corrosion-pit, the size of which can be estimated according to a certain pit-growth law, later to be combined with a crack-growth law to predict a component's corrosion fatigue-life. A comprehensive review of these approaches and their respective limitations was provided by Larrosa *et al* [1]. Most notably, such matters are only relevant if fracture is propelled by the initiation and growth of a single pit, ultimately the point of origin of a primary crack. These types of models might become applicable at later stages of the corrosion fatigue-fracture process, after the emergence of a major crack. However, in most practical cases, the procedure is not necessarily governed by the initiation and growth of a single pit or crack. Typically, the corrosion-fatigue mechanism involves the appearance of multiple pits, mainly at inclusion sites where they serve as local galvanic cells, followed by the pit-growth stage [4-9]. Afterwards, a multiplicity of small fatigue-cracks originates from the pits as stress-concentrators, the interaction and resultant coalescence of which eventually lead to the formation of a significant crack that will dominate fracture [10], [11]. Consequently, an understanding of the multiple-pit initiation/interaction behaviour is essential to the development of a blueprint for forecasting corrosion fatigue-life, based on a more realistic damage scenario.

As the first step towards the establishment of a prediction model, it is necessary to develop a procedure for the quantitative characterization of the spatial distribution of corrosion-pits. In fact, many researchers have applied various spatial statistics techniques, including the Ripley method, Quadrant count, Brix, $\hat{L}$ and Inter-event distance estimators [12-25], to qualitatively characterize corrosion-pit distribution in other practically important localized corrosion research area. Among all the fore-mentioned spatial statistics tools, the Ripley method is widely used, hence it will be discussed briefly here. Ripley method is used to qualitatively determine deviations from complete spatial randomness. It involves the generation of a complete spatial randomness simulation envelope using multiple randomly generated data points of same number as the actual distribution whose spatial distribution is to be determined. The envelope is the plot of the maximum and minimum values of a L_2 statistical function over a range of radii [12]. Next, the values of L_2 function for the actual data points for the same radii range are plotted over the envelope. If this plot falls within the envelope, the distribution is classified as randomly distributed, if it falls above, it is clustered and finally if it falls below, then it is classified as regular. Budiansky et al. [15] applied Ripley method in the study of interactions among pitting sites in AISI 316 stainless steel tested in 0.05M NaCl. They applied this procedure to spatial data of non-metallic inclusions on the specimen surface prior to the corrosion test and to corrosion pits after the test. They observed that the inclusions were randomly distributed while the pits were clustered. Based on this observation, they concluded that the clustering of pit sites is an indication of interactions among localized pitting sites but also warned that the clustering could as well be due to the fact that the non-metallic inclusions from which the pits initiated were initially clustered. Although Ripley method can successfully classify data points as random, clustered or regular, the need to initially generate a complete spatial randomness simulation envelope using large number of randomly generated data points of same number as the actual distribution makes the method computationally expensive for practical usage. Also, for cases where a portion of the line of the L_2 function for the actual data falls within the envelope while other portion falls outside, the classification is no longer straight forward. Furthermore, the method cannot be to quantitatively measure the degree of deviation from complete randomness. The ability to quantitatively measure the deviation from randomness is necessary to develop a probabilistic corrosion fatigue prediction model. To conclude this brief review, the work of Scully et. al [25] merit a mention. Through experiment and model simulation of a stainless steel alloy, they showed that prevention of explosive growth of pits site and clustering of pits can be achieved if the lateral diffusion length, associated with aggressive corrosion products formed at pits, is less than the nearest neighbor distance (NND) of the surface non-metallic inclusions. The NND was taken as the average distance between an inclusion and its five closest neighbors. If the inclusions are randomly distributed or clustered, then this method of estimating NND is practically accurate enough, however if they are a superposition of clustered sets with random set in background, this method of estimation can not be directly used. At first, there is need to separate the clustered sets from the random background. Then NND for each of the cluster sets can be estimated.

In this study, two Nearest-Neighbour Analysis (NNA)-based procedures have been proposed as suitable statistical tools to quantitatively characterize the spatial distribution of corrosion-pits. Using these methods, the spatial distribution of corrosion-pits can be categorized as ordered, random, clustered or consisting of randomly distributed with superimposed clusters. Moreover, it will be shown that, in cases where the corrosion-pit population is a superposition of clusters and a randomly distributed background set, pits belonging to the cluster sets can be identified using an NNA-based technique. The validity of this approach was confirmed by the experimental results for a medium-carbon steel (S45C-JIS, DIN C45, AISI 1045), previously exposed to a mist of 3.5%-NaCl-solution for a duration of 0.5 ~ 6.0 hours. In addition, based on the spatial distribution of non-metallic inclusions on the specimen surfaces, it will be demonstrated that the new method can predict corrosion-pit spatial distribution, especially at the very early stages of the corrosion-process. Finally, about an eventual, corrosion-fatigue prediction model, the practical applications of these procedures are also explored, along with the quality-control of materials exposed to corrosive environments.

2. Analysis

During the 1940s, NNA was developed as a practical tool for characterizing population patterns, propelled by research into the spatial distribution of plants or animals in their natural habitats [26]. The discovery that most populations are not arbitrarily distributed advanced the need for further research, to abandon the simple assumption of haphazard arrangement and to consider the degree of departure from arbitrary distribution [26]. Subsequently, NNA was successfully applied in the fields of materials science, medicine, astronomy, machine-learning, biology and many other disciplines, generally targeted towards the realistic problems associated with the spatial arrangement of certain members of a given population. For example, Shehata and Boyd [27] applied an NNA-based procedure to compare the spatial distribution of non-metallic inclusions on the surfaces of as-cast and as-rolled steels.

The NNA-based method for characterizing the spatial distribution of feature-centroids in planes is herein provided. More complete details can be reviewed in the original publications [26], [28].

Clark and Evans [26] were the first to derive the formulae for calculation of the expected mean, $E(\bar{r}_1)$, and variance of the nearest distance, $E({s_1}^2)$, based on the features of a population, N, being randomly distributed over an area, A, with a distance measurement, r_1, from each feature to its nearest neighbour. When the spatial distribution of features can be considered to be homogeneous, the Poisson-point process, with a density of $\rho = \frac{N}{A}$, $E(\bar{r}_1)$ and $E({s_1}^2)$, are expressed by the following equations:

$$E(\bar{r}_1) = \frac{1}{2\sqrt{\rho}} \tag{1}$$

$$E({s_1}^2) = \frac{4-\pi}{4\pi} \cdot \frac{1}{\rho} \tag{2}$$

where, the observed mean, $\bar{r}_1$, and the variance of r_1, ${s_1}^2$, are formulated as follows:

$$\bar{r}_1 = \frac{\sum r_1}{N} \tag{3}$$

$${s_1}^2 = \frac{\sum(r_1 - \bar{r}_1)^2}{N} \tag{4}$$

Using Equations (1)~(4), a simple method for categorizing the spatial distribution of a plane's features can be derived as follows: If Q is defined as the ratio of the observed and expected means, $Q = \bar{r}_1/E(\bar{r}_1)$, with R being the ratio of observed and expected variance, $R = {s_1}^2/E({s_1}^2)$. The featured populations can be classified as random, regular or clustered sets, or as clusters superimposed onto random backgrounds, via the following associations of Q and R:

- Random sets $\quad Q = 1, \quad R = 1$

- Regular sets $Q > 1, \quad R \ll 1$
- Clustered sets $Q < 1, \quad R < 1$
- Clustered, with a superimposed background $Q < 1, \quad R > 1$

If the Q value indicates a non-random distribution of a set (*i.e.*, $Q \neq 1$), it then becomes necessary to measure the relevance of the $\bar{r}_1$ departure from $E(\bar{r}_1)$, in order to quantify the reliability of this procedure. Clark and Evans [26] also developed a significance test based on the normal curve. In an arbitrarily distributed population with the same ρ and N as those of the observed population, the equation for calculating the standard error of mean distance to the nearest neighbour, $\sigma_{E(\bar{r}_1)}$, is provided as follows:

$$\sigma_{E(\bar{r}_1)} = \frac{0.26136}{\sqrt{N\rho}} \tag{5}$$

Then, the standard variant of the normal curve, c, is offered by the ensuing equation:

$$c = \frac{\bar{r}_1 - E(\bar{r}_1)}{\sigma_{E(\bar{r}_1)}} \tag{6}$$

Using the calculated c value, in combination with a suitable table for normal distribution, the level of significant deviation can thus be established. In this paper, in order to differentiate between the afore-mentioned procedure and other distance-based methods (*e.g.*, the Ripley, Brix, $\hat{L}$ estimator, Inter-event distance estimator, it is labelled herein, the *QR* method. Compared to others, key advantages of the *QR* method include its simplicity, ease of interpretation and quantitative incorporation of the degree of departure from random distribution.

Schwarz and Exner [28] developed a procedure for separating cases where feature-populations involved clusters with overlapping backgrounds. By considering a compound set to comparably be an overlay of a very dense, Poisson-point process (cluster-sets) and a relatively less-dense, homogenous Poisson-point method (background-sets), a practical and simple rule was developed to determine which feature belonged to either the cluster- or background-sets. According to that procedure, r_1* and r_2* were defined by the successive equations:

$$r_1{}^* = \left[\frac{1}{\pi(\rho_{c1} - \rho_{b1})} ln\left(\frac{c_1}{1 - c_1} \cdot \frac{\rho_{c1}}{\rho_{b1}}\right)\right]^{1/2} \tag{7}$$

$$r_2{}^* = \left[\frac{1}{\pi(\rho_{c2} - \rho_{b2})} ln\left(\frac{c_2}{1 - c_2} \cdot \frac{\rho_{c2}{}^2}{\rho_{b2}{}^2}\right)\right]^{1/2} \tag{8}$$

where, $c_1, \rho_{c1}, \rho_{b1}$ and $c_2, \rho_{c2}, \rho_{b2}$ are obtained from the complete solution of Equation (9) and (10), accordingly:

$$\frac{c_1}{\sqrt{\rho_{c1}}} + \frac{1-c_1}{\sqrt{\rho_{b1}}} = 2M_1^1 \tag{9a}$$

$$\frac{c_1}{\rho_{c1}} + \frac{1-c_1}{\rho_{b1}} = \pi M_2^1 \tag{9b}$$

$$\frac{c_1}{\sqrt{\rho_{c1}}^3} + \frac{1-c_1}{\sqrt{\rho_{b1}}^3} = \frac{4\pi}{3} M_3^1 \tag{9c}$$

$$\frac{c_2}{\sqrt{\rho_{c2}}} + \frac{1-c_2}{\sqrt{\rho_{b2}}} = \frac{4}{2} M_1^2 \tag{10a}$$

$$\frac{c_2}{\rho_{c2}} + \frac{1-c_2}{\rho_{b2}} = \frac{\pi}{2} M_2^2 \tag{10b}$$

$$\frac{c_2}{\sqrt{\rho_{c2}}^3} + \frac{1-c_2}{\sqrt{\rho_{b2}}^3} = \frac{8\pi}{15} M_3^2 \tag{10c}$$

where, M_1^1, M_2^1 and M_3^1 are the observed first-three moments of the nearest-neighbors, whereas, M_1^2, M_2^2 and M_3^2 are the observed first-three moments of the second-nearest neighbors. Insofar as a specific point is concerned (feature-centroid), if the distance to its nearest-neighbour point, r_1, is larger than $r_1{}^*$, and the distance to its second nearest-neighbour point, r_2, is greater than $r_2{}^*$, then the point is classified as belonging to background-sets. The procedure is labelled herein, the Schwarz method.

3. Material and methods

The material selected for this study was a hot-rolled, medium-carbon, JIS-S45C steel (equivalent to DIN C45 and AISI 1045), very often used in the fabrication of machined engineering parts. Its chemical composition and mechanical properties are outlined in Tables 1 and 2, respectively. Specimens were 120 mm-long, 24 mm-wide and 1 mm-thick, extracted from the center of a 25-mm-diameter cylindrical bar. The longitudinal direction of the specimens was parallel to the rolling-direction of the base-material. One side of the specimen was mirror-polished, in conformity with the procedure proposed by Samules [29] for the removal of machined layers beneath specimen-surfaces, as part-preparation for the microscopic inspection of inclusions. The polishing process is detailed in Figure 1.

Prior to corrosion-testing, the unpolished sides of specimens, as well as all edges, were covered with Teflon tape, in order to inhibit the corrosion process. The Neutral Salt Spray Test (NSST) was then introduced as a corrosion-testing method, in accordance with JIS Z 2371 (ISO 9227:2017), and a test-solution of 3.5%-NaCl with a 7.0 pH value was selected. To ensure that the pH value did not vary, it was measured both before and after testing. The temperature inside the chamber was maintained at 35°C. To investigate the evolution of pit spatial distribution in relation to time, four specimens were exposed to a corrosive environment for 0.5, 2.0, 4.0 or 6.0 hours, as documented in Table 3. Hereafter, the uncorroded specimen is identified as S45-0, with the corroded specimens accordingly labelled as S45-0.5, S45-2.0, S45-4.0 and S45-6.0, based on their respective exposure-times. At the outset of the tests, all specimens (except S45-0) were placed in the chamber, with each specimen removed when its individual exposure-time had been attained. Specimen S45-0 was especially reserved for inclusion in the spatial-distribution analysis. After corrosion-testing, specimen surfaces were again mirror-polished, to remove any rust which might have rendered the microscopic pit-observation rather difficult. During the polishing process, extreme care was taken to ensure that the initiated pits had been buffed adequately.

The progress of pit spatial distribution was subsequently observed by means of optical microscopy (OM) and scanning electron microscopy (SEM). The chemical compositions of inclusions in some specimens were identified via energy-dispersive, X-ray spectroscopy (EDX), at an acceleration voltage of 20 kV. Figure 2 showcases the SEM inclusion-images at a higher magnification and at the corresponding EDX spectrum, primarily highlighting two inclusion types, *i.e.,* MnS and Ca-Mn-S. The MnS-size was relatively larger than that of the Ca-Mn-S, with the quantity of MnS superior to that of Ca-Mn-S. Spatial distribution was quantified by OM image-analysis, for which the inspection area was defined as 10×10 mm^2. The coordinate of each pit-centroid was recorded for all visible pits and reconstructed for the later pit spatial-distribution analysis.

4. Results and discussion

The corroded specimen-surfaces, after exposure to the corrosive environment, are displayed in Figure 3. Following corrosion-testing, rusted specimen-surfaces were rinsed in de-oxygenated water, later dried using a hot-air jet. Afterwards, mechanical-polishing was employed to remove rust and to prepare specimens for OM-observation. Figure 4 displays examples of the polished S45-0.5 (exposure-time of 0.5 hours) and S45-

6.0 (exposure-time of 6.0 hours) specimen-surfaces, after removal of corrosion-rust. While it was noted that corrosion-pits developed in large quantities at 0.5 hours, some individual pits did not really grow as much between 0.5 ~ 6.0 hours. A significant escalation in size occurred predominantly through coalescence with neighboring pits, the evidence of which can be verified via examination of the pit-shape in Figure 4 (b). In fact, the coalescence of pits was already evident from as early as 0.5 hours (*cf.* Figure 4 (a)) and rather obvious from 6.0 hours (*cf.* Figure 4 (b)). Moreover, some coalesced-pits appeared to be elongated, that is, parallel to the rolling-direction of the material.

In order to observe if there is influence of the underlying material microstructural phases on the observed pits and establish the mode of the corrosion that occurred, specimen S45-0.5 was etched with 3% Nital for 6 seconds to prepare it for microstructural observation. Figure 5 shows that the underlying material microstructure is combination of ferrite and pearlite phases. Corrosion pits can be found in both phases as well as at their boundaries. This suggest that the observed pits are not due to a phase type dissolving in another nor due to dissolution at phase boundaries. It remains to show that the inclusions on the specimen surfaces play a key role in the pit initiation process. To demonstrate this, specimen S45-0, which was reserved for inclusion inspection, was exposed to the corrosion chamber for about 5 mins. For this exposure time, there was no need for polishing after the exposure, this is because general corrosion has not occurred. Only localized corrosion at some certain location can be seen. Thus, with this specimen it will be possible to observe the role played by the inclusions in the locations where localized corrosion initiated. In Figure 6, it can be observed that each one of the locations where localized corrosion initiated is associated with an inclusion or cluster of inclusions in their vicinity. Wranglen [4] has provided comprehensive theoretical explanation of the mechanism by which localized corrosion initiate and propagate in the vicinity of inclusions, especially sulphides. The work of Ryan et. al [7] is also another excellent work on this topic.

Figure 7 displays a reconstructed demonstration of the spatial location of features(inclusions/pits), with each point representing a feature-centroid within the inspection area. Coordinates were normalized according to the length of the review area and, based on the data, the distances between all feature-pairs were calculated. Subsequently, according to the arrangement of each feature in ascending order of the appraised gaps, the spaces between the nearest and second-nearest neighbors were recorded.

In terms of the quantitative characterization of the spatial distribution of features, both the equations and the QR method were programmed into a MATLAB code and applied to the test data. The major parameter outputs are listed in Table 4. Similarly, the Schwarz method was incorporated into a MATLAB code, to identify features belonging to cluster-sets. Consequently, regarding specimen S45-0, $Q = 0.77$ and $R = 2.15$, this demonstrates that the inclusion-population is clustered with a superimposed background-set. According to the Q value of 0.77, the nearest neighbors are, on average, 0.77 times further apart than would have been expected, if inclusions had been distributed arbitrarily. Figure 8 (a) presents the inclusion-centroids associated with cluster-sets (as depicted by red dots), in addition to background-sets (represented in blue). The result suggests that 79% of inclusions relate to cluster-sets. Shehata *et al.* also detected the inclusion-population, spatially distributed as cluster-sets against a random background on the polished surface of a Ti-V micro-alloyed steel [27]. They attributed the formation of clusters to the breaking and fragmentation of large inclusions during a material's manufacturing rolling-process. When the steel matrix becomes heavily deformed during the rolling-process, inclusions will split into small fragments. However, it should be noted that this is not the only mechanism governing the formation of inclusion-clusters. Since most clusters appear to be arranged linearly, parallel to the rolling-direction of the material, it has therefore been suggested that the rolling-process may play a role in their formation. As the cluster-sets account for a large portion of the inclusion population, they are expected to play a crucial role in the spatial distribution of corrosion-pits. In addition, the shape of the cluster arrangement will strongly influence the pit-shape formed by the coalescence of neighboring pits. This issue will later be discussed in detail.

The (Q, R) values were, respectively,$(0.74, 2.10)$, $(0.81, 2.33)$, $(0.82, 2.17)$ and $(0.87, 1.92)$, for the specimens S45-0.5, S45-2.0, S45-4.0 and S45-6.0. This data implies that their arrangement was in cluster-sets against an overlapping background. The pit-centroids belonging to the cluster-set identified by red dots, with the background set identified in blue, are both illustrated in Figs. 7 (b-e). The Q value for the pit-population, as seen on S45-0.5 ($Q = 0.74$), very closely approximates that of the inclusion-distribution of S45-0 ($Q = 0.77$). Despite the two datasets being obtained from different specimens, the divergence remains less than 4%. Such a result confirms the possibility of predicting the spatial distribution of pits from the outset of corrosion, based on the inclusion-data registered from specimen-surfaces prior to the onset of corrosion. The reason for the compelling correlation between inclusion-population arrangement and corrosion-pits is that most corrosion-pits launch at/near inclusion-sites. This occurrence has already been acknowledged by materials science researchers [4-7], whilst never having yet been used to foretell the pit-population arrangement at the outset of the corrosion process. Furthermore, within the context of exposure-time to a corrosive environment, Figure 9 details the evolution of the Q value, surging from 0.74 to 0.87 within a timeframe of 0.5 ~ 6 hours. Such an event indicates that the increase in exposure-time results in changes to the spatial distribution of corrosion-pits, ranging from randomly distributed clusters with superimposed background-sets to non-homogeneous random distribution. This change is primarily due to the coalescence of corrosion-pits, in close-enough proximity to form larger pits.

Cawley and Harlow [30] attempted to characterize the spatial distribution of inclusions on the surface of a 2024-T3 aluminum alloy and its corrosion-pits, after exposure to a 0.5M- (3.5%)-NaCl environment for 10 ~ 72 hours. Qualitative characterization was accomplished by comparison of the second, reduced-moment function of inclusion/corrosion-pit centroids, $K(t)$, within the anticipated secondary, reduced-moment function of the complete spatial-randomness (CSR) model. Figure 10 presents $K(t)$, along with experimental data for inclusions and corrosion as functions of *t*, where *t* is the distance between the centroids of inclusion-/corrosion-pits [21]. Since the estimated, corrosion-pit data curves all fell below the diagonal line of the CSR model, it was presumed that the pit-centroids had been distributed regularly. Furthermore, since most portions of the estimated inclusion-data curve fell above the diagonal line of the CSR model, it was inferred that the inclusion-centroids displayed a cluster-type distribution. The approach by Cawley *et al.* is similar in principle to the QR method. The diagonal line of the CSR model is equivalent to $Q = 1$, whereby the curve that shifts above and below the diagonal line corresponds to $Q < 1$ and $Q > 1$, respectively. From such a viewpoint, it appears that Cawley *et al.* accurately classified the spatial corrosion-pit distribution as an evolution into something perfectly regular that corresponds with time. In Figure 10, the estimated pit-curves shift further away from the diagonal straight-line, with an increase in corrosion-time corresponding to a heightened value of Q. However, the inclusions data was merely classified as clustered sets, which might not necessarily be correct. More correct classification for the inclusions can be cluster sets with superimposed background set. Namely, if all the portion of the estimated curve for the inclusions lies above the diagonal line then the data can be classified as cluster sets, but if some part of the curve lies above the diagonal line and the other part below it (see the data for "as polished: 216 particle" in Figure 10), it is more appropriate to classify them as cluster sets with superimposed background set. However, Cawley and Harlow attributed the section of the estimated inclusion-data curve situated below the diagonal line of the CSR model to measurement limitations of the microscope used. By employing a quantitative approach (*e.g.*, the QR method), such a classification error could be avoided - a definite advantage of the proposed technique.

5. Practical Applications

5.1. Material-quality problem

Used for the quality-control of materials, the conventional standards for inclusion-rating (*i.e.*, ISO 4967, JIS-G-0555, ASTM E45 and DIN 50602) focus primarily on the shape, density and size of inclusions, in order to determine the cleanliness index of metal samples. Although those guidelines may be appropriate for materials to be used in air, they are not suitable for those destined for use in corrosive environments, where pitting is the driving force behind most failure mechanisms. This is because the spatial distribution of inclusions plays a more crucial role in corrosion pit-arrangement/-growth [14-25], as opposed to size. Once pits initiate at/near inclusion-sites, their growth is driven mainly by coalescence with neighboring pits. This phenomenon should be considered for inclusion-rating, especially when the materials are destined for corrosive environments. Therefore, a combination of the QR and Schwarz methods is proposed as a novel, inclusion-rating system. According to the QR process, for example, if a Batch A sample is recorded as $Q = 0.93$ and one from Batch B is $Q = 0.65$, Batch B would consequently be expected to be more clustered than Batch A. If samples from both Batches A and B were to be placed in identical corrosive environments for an equivalent period of exposure, the Batch B sample would be expected to generate larger corrosion-pits. Therefore, Batch A could be judged to be cleaner than Batch B. Additionally, in cases where Q and R values are close for both batches, the Schwarz method can additionally be used to identify inclusions belonging to the cluster sets for further analysis. Moreover, by analyzing the shape of the cluster sets, very important deduction can be made. For example, let us presume that batch A contains cluster sets that are mostly circular in shape while batch B contains cluster sets that are mostly arranged in a line perpendicular to loading direction. The former can be judged as superior in view of corrosion fatigue strength. This is because if we regard their resulting coalesced pits as mechanically-equivalent to small cracks, as proposed by Murakami [22], the projected area of coalesced pit from batch B will be larger than batch A, as a result, the stress intensity of coalesced pits from batch B will be larger than batch A.

5.2. Corrosion-fatigue prediction model

Larrosa *et al.* [3] comprehensively reviewed several models for the prediction of corrosion fatigue-strength in machines and structures subjected to cyclic-loading in corrosive environments, the main limitations of which were already explored in the introductory section of this paper. Although essentially quite thorough, a major theory proposed by Kitagawa *et al.* [10] was nevertheless overlooked in the Larrosa investigation. In fact, the Kitagawa approach to the problem of corrosion fatigue-strength seems to be the most appropriate, based on the actual mechanism of corrosion-fatigue failure. The Kitagawa model (KM) involves the statistical simulation of numerous distributed cracks, while also accounting for the interaction effect of their Stress Intensity Factors (SIFs), the simulation variables being the sizes and spatial locations of cracks. However, from a practical standpoint, there are four key limitations to the KM: (i) the spatial-distribution parameters of corrosion fatigue-cracks must be identified prior to simulation; (ii) the size-distribution criteria of corrosion-fatigue cracks need to be understood before replication; (iii) the crack-propagation stage is not included; (iv) during the SIF computation of cracks, the interaction factors of two-dimensional cracks in an infinite plate are to be used, as opposed to those of multiple, three-dimensional surface cracks. These limitations must first be addressed to ensure that the KM is useful to engineers during the design stage of components to be used in corrosive environments, most of the necessary input data (*e.g.*, size and spatial distribution of corrosion-pits) not being available at the outset.

To experimentally validate KM, Kitagawa *et al.* [10] performed corrosion-fatigue tests on a high-strength steel plate with a tensile strength of $\sigma_{\mathrm{UTS}} = 530$ MPa. The stress ratio and test frequency were 0.04 and 10 Hz, respectively. The corrosive environment was distilled water, with a pH value ranging from 5.6 ~ 6.0, run at a flowrate of $0.25\ \mathrm{cm}^3/\mathrm{s}$.

Initially proposed by Masuko *et al.* [32], the Homogeneity function method was applied by Kitagawa *et al.* to determine the spatial distribution of cracks for statistical simulation. Based on the Masuko concept, the degree of departure of a population's spatial distribution from an ideal homogeneous arrangement, D, can be determined by subtracting the H value of a uniformly-random distribution, H_{random}, from that of the population, $H_{\mathrm{population}}$. The formulae for the calculation of H can be found in [10], [32]. In principle, the D value in the Homogeneity function method is similar to the Q value in the QR method: $D = 0$ corresponds to $Q = 1$, both indicating that the population is an ideal uniformly random distribution. Likewise, $D > 0$ is equivalent to $Q > 1$, both implying a deviation from ideal randomness towards regularity. However, a difference emerges in the case where $D < 0$ (*i.e.*, $Q < 1$). According to the Homogeneity function method, a negative D value implies a deviation from ideal randomness towards clustering. Nevertheless, the Homogeneity function method cannot differentiate between regular cluster sets and those with a superimposed background distribution, since both scenarios register $D < 0$. On the other hand, using the R value via the QR approach, one can separate between the two.

A test result from the Kitagawa study [10] is presented in Figure 11. The figure displays the spatial distribution of corrosion-pits and cracks on a specimen surface, at a stress range of 235 MPa after 1×10^6 cycles. $H_{population}$ and H_{random} figures were respectively reported to be 8.4039 and 8.5608, corresponding to the D value of -0.0569. However, cracks were still classified according to uniform-random distribution. Since the inherent difference between them was small, Kitagawa *et al.* argued that both H values could be considered equal, *i.e.*, $D = 0$. However, this premise may not be acceptable, since even a D value of -0.008 is enough to classify a distribution as "clustered", according to the Homogeneity function method [32].

In most practical cases, since the distribution of inclusions and corrosion-pits often stem from the superposition of clusters and incidental background-sets, the QR method is deemed to be the most appropriate. Furthermore, based on the observations recorded in this study, it is proposed that in the KM-context, the spatial distribution of inclusions be substituted for that of corrosion fatigue-cracks, thereby providing a solution to the first, afore-mentioned limitation. Information about the spatial distribution of inclusions in materials can be obtained by following the experimental procedures outlined in this study. Further investigations into the other three identified drawbacks are of critical import, if a model for the prediction of corrosion fatigue-strength is to be developed based on the fracture-process and will feature in our future research.

6. Conclusions

Based on the results of corrosion-testing and the statistical analyses conducted during this study, the following conclusions were established:

(1) The exposure of JIS-S45C to a 3.5%-NaCl-solution-mist for up to six hours resulted in the introduction of numerous corrosion-pits, quite early in the corrosion process. The pits initiated primarily at non-metallic inclusion-sites. While an increase in exposure-time did not significantly alter individual pit-size, the number of pits was amplified, resulting in pit growth by coalescence of pits that form clusters.

(2) A Nearest-Neighbour Analysis (NNA)-based procedure, identified as the QR method, was applied to quantitatively characterize the spatial distribution of inclusions and corrosion-pits on specimen surfaces. Depending on the respective values of Q and R, the featured surface-populations were classified as

random, clustered or regular sets, or clusters with superimposed backgrounds, the latter category applying to the spatial distribution of inclusions. In the early stages of corrosion, the pit-arrangement resembled that of the surface-inclusions, becoming more randomly distributed as corrosion progressed, with the coalescence of clustered pits primarily attributed to this phase.

(3) Another NNA-based procedure known as the Schwartz method was introduced to identify clusters of inclusions, or pits from background-sets.

(4) The combined QR /Schwartz approach was suggested as a novel procedure for inclusion-rating and quality-checking of materials destined for use in corrosive environments. These techniques have tremendous potential for determining the spatial distribution of corrosion fatigue-cracks, using fracture mechanics-based, corrosion-fatigue, strength-prediction models such as those proposed by Kitagawa *et al.* and Harlow *et al.*[33]

Funding

This research did not receive any specific grant from funding agencies in the public, commercial, or not-for-profit sectors.

Declarations of interest

None

Data Availability

The raw data required to reproduce these findings are available to download from [The raw data required to reproduce these findings cannot be shared at this time as the data also forms part of an ongoing study]. The processed data required to reproduce these findings are available to download from [The processed data required to reproduce these findings cannot be shared at this time as the data also forms part of an ongoing study].

References

[1] D.J. McAdam Jr., Fatigue and Corrosion Fatigue of Metals, Proc. Int. Cong. Testing Materials 1, 305 (1927).

[2] S. Kawai, K. Kasai, Consideration of allowable stress of corrosion fatigue (focused on the influence of pitting), Fatigue Fract. Engng. Mater. 8 (1985) 115−127.

[3] N.O. Larrosa, R. Akid, R.A. Ainsworth, Corrosion-fatigue: a review of damage tolerance models, International Materials Review. 63 (2018) 283−308.

[4] G. Wranglen, Pitting and Sulphide inclusions in steel, Corrosion Sci. 14 (1974) 331−349.

[5] M.A. Baker, J.E. Castle, The initiation of pitting corrosion at MnS inclusions, Corrosion Sci. 34 (1993) 667−682.

[6] C. Punckt, M. Bölscher, H.H. Rotermund, A.S. Mikhailov, L. Organ, N. Budiansky, J.R. Scully, J.L. Hudson, Sudden onset of pitting corrosion on stainless steel as a critical phenomenon, Science. 305 (2004) 1133−1136.

[7] M.P. Ryan, D.E. Williams, R.J. Chater, B.M. Hutton, D.S. McPhail, Why stainless steel corrodes, Nature. 415 (2002) 770−774.

[8] M.D. McMurtrey, D.E. Mills, J.T. Burns, The effect of pit size and density on the fatigue behaviour of a pre-corroded martensitic stainless steel, Fatig. Fract. Eng. Mater. Struct. 42 (2019) 3−18.

[9] D.G. Harlow, Constituent Particle Clustering and Pitting Corrosion, Metall. Mater. Trans. A. 43 (2012) 2832−2838.

[10] H. Kitagawa, T. Fujita, K. Miyazawa, Small Randomly Distributed Cracks in Corrosion Fatigue, Corrosion-Fatigue Technology, ASTM STP. 642 (1978) 98−114.

[11] A. Boukerrou and R.A. Cottis, Crack Initiation in the corrosion fatigue of structural steels in salt solutions, Corrosion Sci. 35 (1993) 577−585.

[12] P.J. Diggle, Statistical Analysis of Spatial Point Patterns, Academic Press, 1983.

[13] M. Reuter, K.E. Heusler, Statistical Investigations of the Pitting of Passive Iron, Electrochimica Acta. 35 (1990) 1809−1814.

[14] J. López De La Cruz, S.P. Kuniewski, J.M. Van Noortwijk, M.A. Gutiérrez, Spatial Nonhomogeneous Poisson Process in Corrosion Management, J. Electrochem. Soc. 155 (2008) C396−C406.

[15] N.D. Budiansky, L. Organ, J.L. Hudson, J.R. Scully, Detection of interactions among localised pitting sites on stainless steel using spatial statistics, J. Electrochem. Soc. 152 (2005) B152−B160.

[16] J. López De La Cruz, M.A. Gutiérrez, Spatial statistics of pitting corrosion patterning: Quadrant counts and the non-homogeneous Poisson process, Corrosion Sci. 50 (2008) 1441−1448.

[17] B. Wu, J.R. Scully, J.L. Hudson, Cooperative Stochastic Behavior in Localized Corrosion: I. Model, J. Electrochem. Soc. 144 (1997) 1614.

[18] T. T. Lunt, T. Pride, J.R. Scully, J.L. Hudson, Cooperative Stochastic Behavior in Localized Corrosion: II. Experiments, J. Electrochem. Soc. 144 (1997) 1620.

[19] T. T. Lunt, J.R. Scully, V. Brusamarello, A. S. Mikhailov, J. L. Hudson, Spatial Interactions among Localized Corrosion Sites: Experiments and Modelling, J. Electrochem. Soc. 149 (2002) B163.

[20] N.D. Budiansky, J.L. Hudson, J.R. Scully, Origins of Persistent Interaction among Localized Corrosion Sites on Stainless Steel, J. Electrochem. Soc. 151 (2004) B233.

[21] L. Organ, J.R. Scully, A.S. Mikhailov, J.L. Hudson, A Spatiotemporal model of interactions among metastable pits and the transition to pitting corrosion, Electrochim. Acta 51 (2005) 225-241.

[22] L. Organ, Y. Tiwary, J.R. Scully, A.S. Mikhailov, J.L. Hudson, Interactions among metastable pits on heterogenous electrodes, Electrochim. Acta 3 (2007) 873-885.

[23] S. Jain, M.L.C. Lim, J.L. Hudson, J.R. Scully, Spreading of intergranular corrosion on the surfaces of sensitized Al-4.4Mg alloys: a general finding, Corros. Sci. 59 (2012) 136-147.

[24] S. Jain, J.L. Hudson, J.R. Scully, Effects of constituent particles and sensitization on surface spreading of intergranular corrosion on a sensitized AA5083 alloy, Electrochim. Acta 108 (2013) 253-264.

[25] J.R Scully, N.D. Budiansky, Y. Tiwary, A.S. Mikhailov, J.L. Hudson, An alternative explanation for the abrupt increase at the pitting potential, Corros. Sci. 50 (2008) 316-324.

[26] P.J. Clark, F.C. Evans, Distance to nearest neighbour as a measure of spatial relationships in population, Ecology. 35 (1954) 445−453.

[27] M.T. Shehata, J.D. Boyd, Measurement of spatial distribution of inclusions, Inclusions and their influence on material behaviours, ASM International (1988) 123−131.

[28] H. Schwartz, H.E. Exner, The characterization of the arrangement of feature centroids in planes and volumes, J. Microscopy. 129 (1983) 155−169.

[29] L.E. Samuels, Metallographic Polishing by Mechanical Means, Sir Isaac Pitman & Sons Ltd., Melbourne & London, 1967.

[30] N.R. Cawley, D.G. Harlow, Spatial statistics of particles and corrosion pits in 2024-T3 aluminum alloy, J. Mater. Sci. 31 (1996) 5127−5134.

[31] Y. Murakami, Metal Fatigue: Effects of Small Defects and Nonmetallic Inclusions, Elsevier, Oxford, UK, 2002.

[32] H. Kawarada, N. Masuko, H. Yamanagida, Journal of the Faculty of Engineering, University of Tokyo. 31 (1972).

[33] D.G. Harlow, R.P. Wei, A probability model for the growth of corrosion pits in aluminum alloys induced by constituent particles, Engineering Fracture Mechanics. 59 (1998) 305-325.

Figures

240-SiC-paper ➡ 400-SiC-paper ➡ 9-μm-Diamond paste ➡ 3-μm-Diamond paste

Figure 1. Procedure for mechanical polishing.

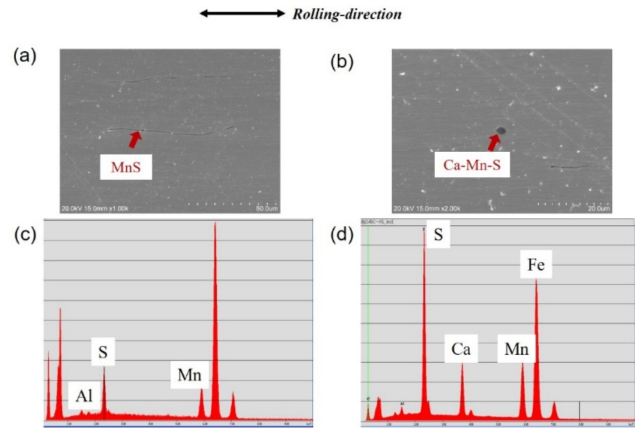

Figure 2. The SEM micrographs of two types of corrosion-free inclusions in a JIS-S45C steel are presented in (a) and (b). EDX spectra of the same are reproduced in (c) and (d). Inclusions shown in (a) and (b) were determined to be MnS and Ca-Mn-S, respectively.

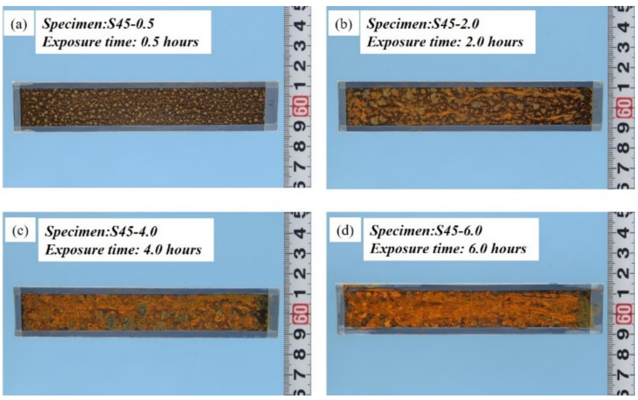

Figure 3. The corroded surfaces of JIS-S45C specimens, after exposure to 3.5%-NaCl for (a) 0.5, (b) 2.0, (c) 4.0 and (d) 6.0 hours at 35°C.

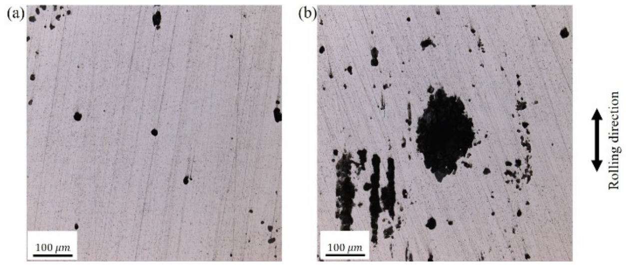

Figure 4. Corrosion pits on the surfaces of JIS-S45C specimens, after exposure to 3.5%-NaCl for (a) 0.5 and (b) 6.0 hours at 35°C. The rolling-direction appeared to play a crucial role in the shaping and formation of coalesced pits.

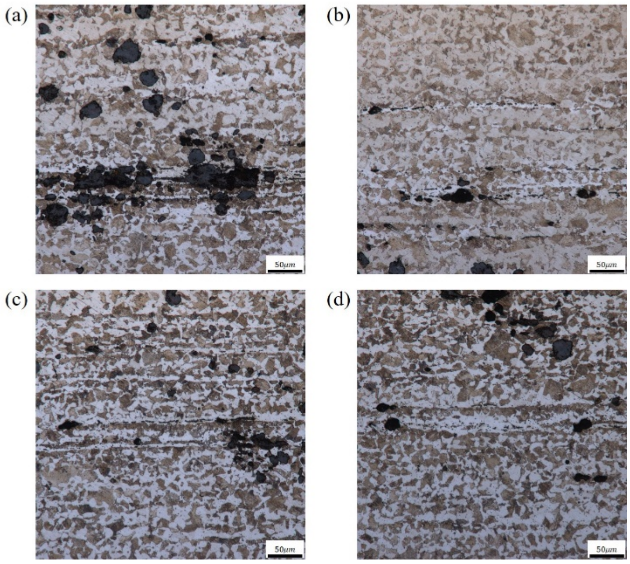

Figure 5. Corrosion pits on the surface of specimen S45-0.5. Pits nucleated at both ferrite and pearlite phases, as well as at their boundaries. (a) – (d) are randomly selected locations on the specimen surface.

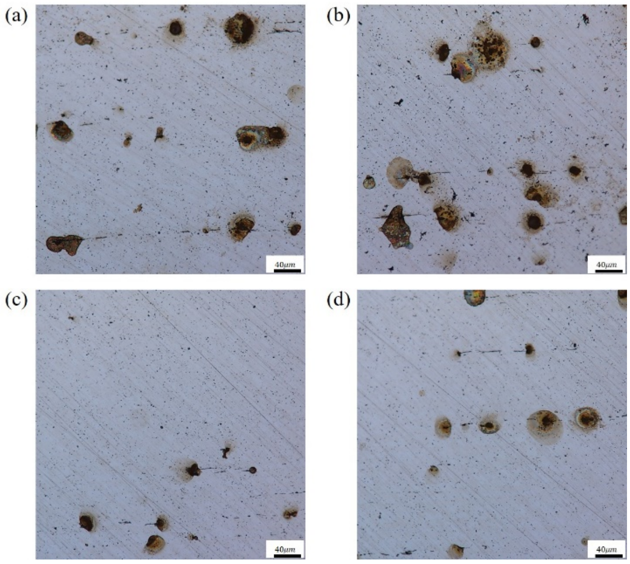

Figure 6. Locations where localized corrosion and pitting occurred on the surface of specimen S45-0. An inclusion or cluster of inclusions can be seen at each of the locations where localized corrosion occurred. (a) – (d) are randomly selected locations on the specimen surface.

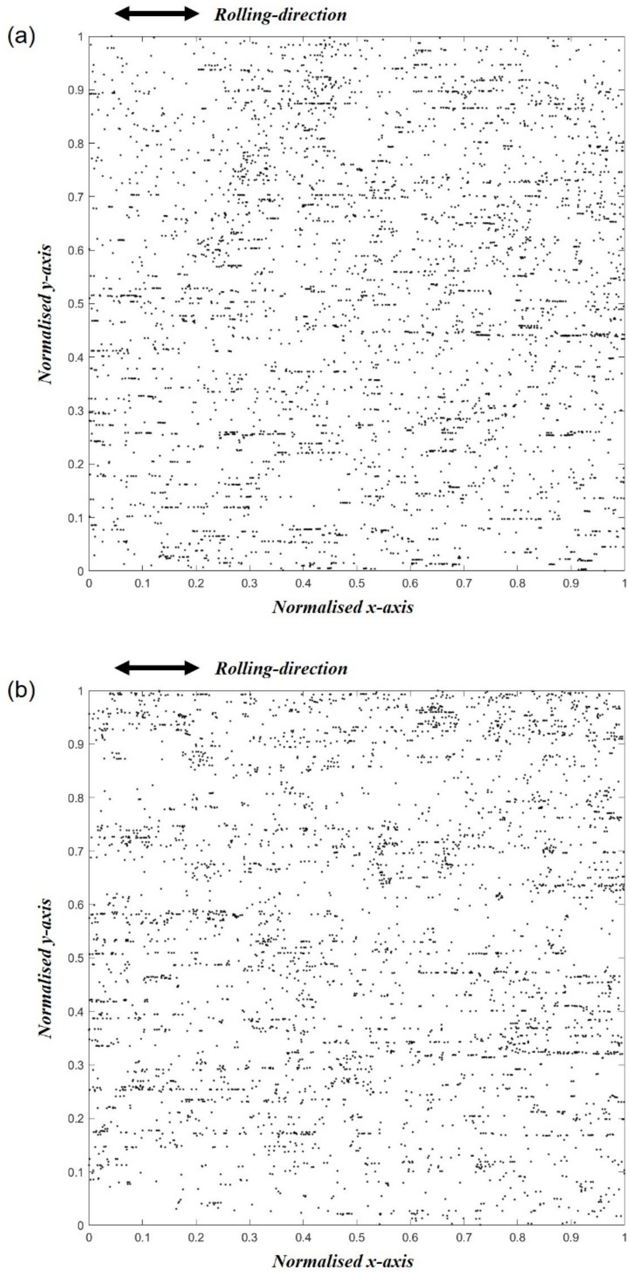
Rolling-direction
(a)
Normalised y-axis
Normalised x-axis
Rolling-direction
(b)
Normalised y-axis
Normalised x-axis

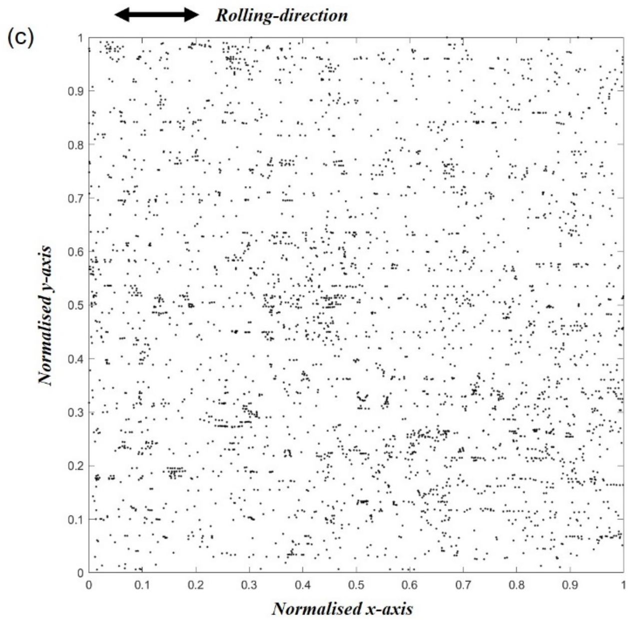
Rolling-direction
(c)
Normalised y-axis
Normalised x-axis
0
0.1
0.2
0.3
0.4
0.5
0.6
0.7
0.8
0.9
1

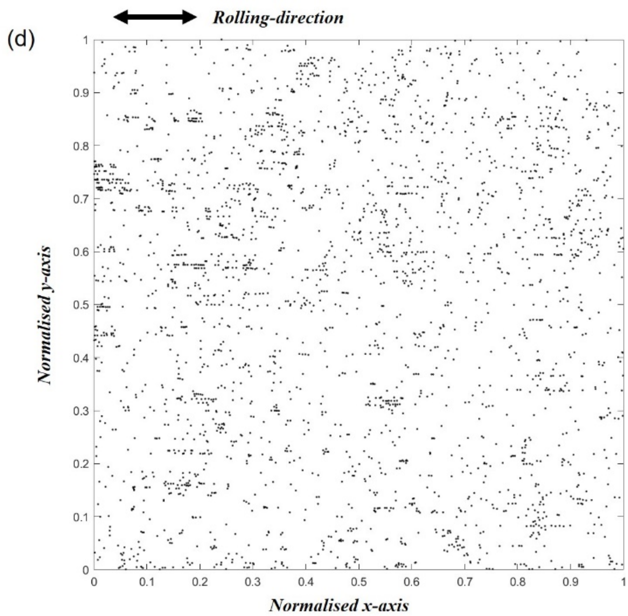
Rolling-direction
(d)
Normalised y-axis
Normalised x-axis
0
0.1
0.2
0.3
0.4
0.5
0.6
0.7
0.8
0.9
1

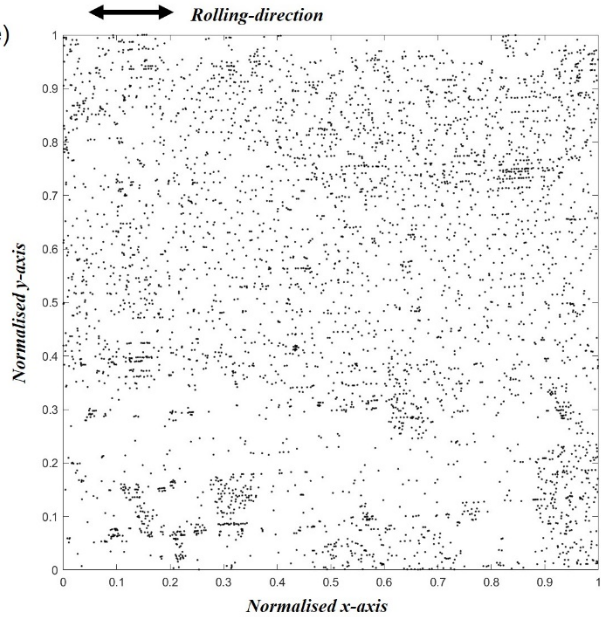

Figure 7. Reconstructed, centroid spatial-distribution of (a) inclusions in S45-0, (b) pits in S45-0.5, (c) pits in S45-2.0, (d) pits in S45-4.0 and (e) pits in S45-6.0.

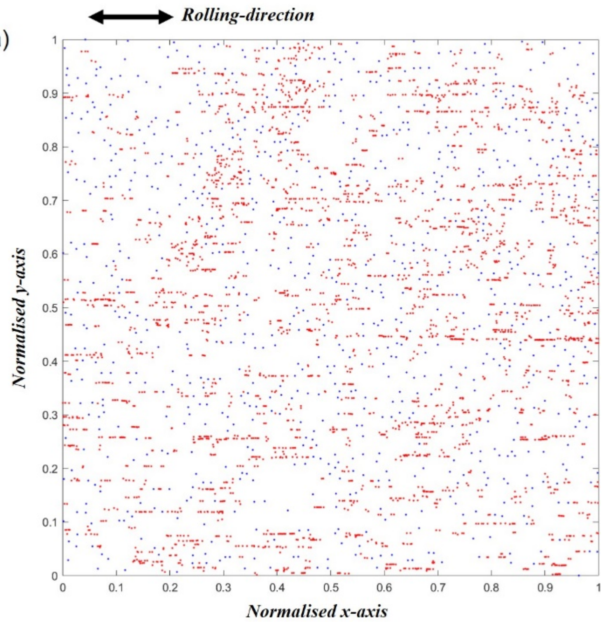

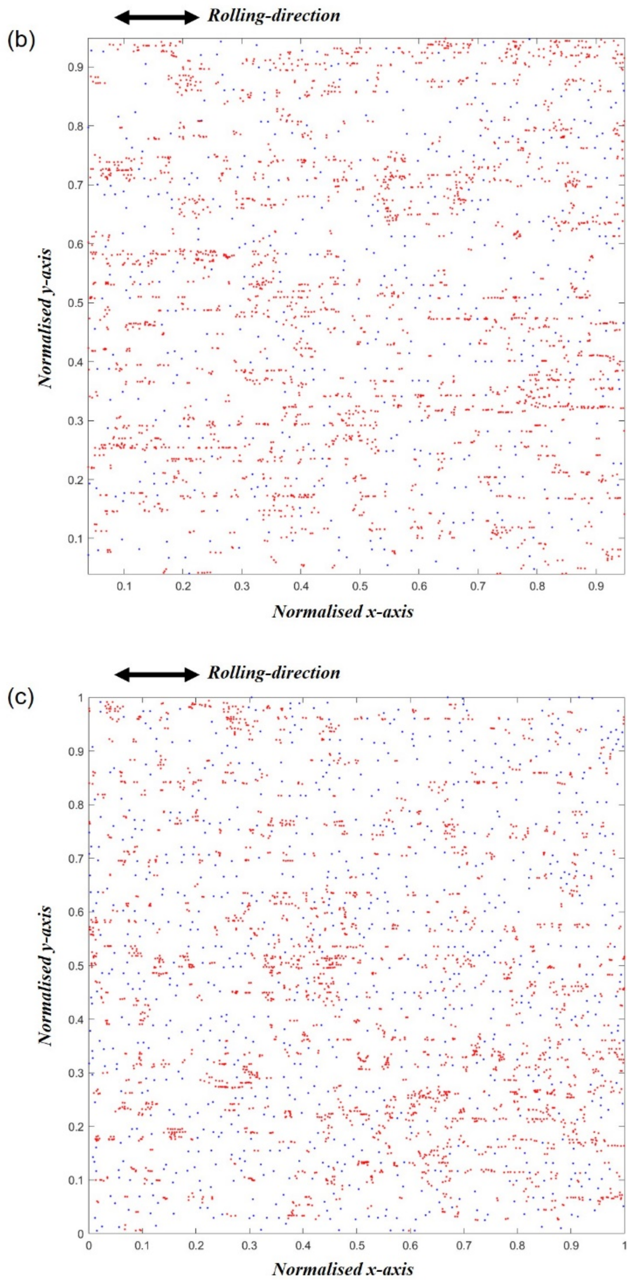
Rolling-direction
(b)
Normalised y-axis
Normalised x-axis
Rolling-direction
(c)
Normalised y-axis
Normalised x-axis

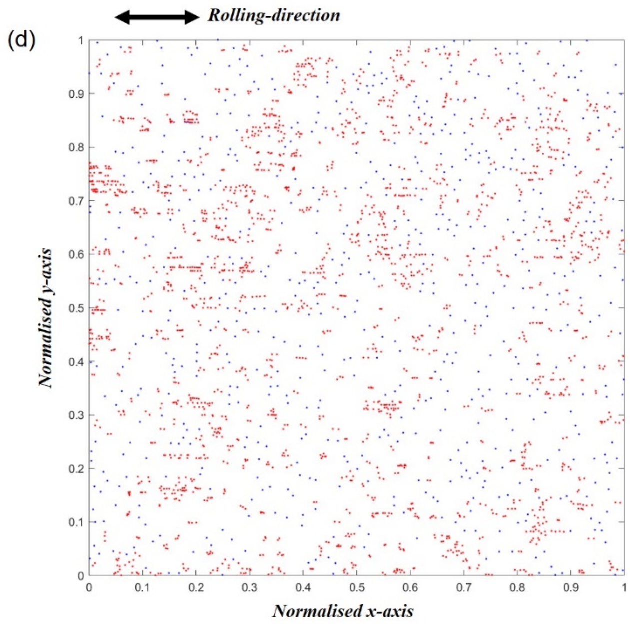

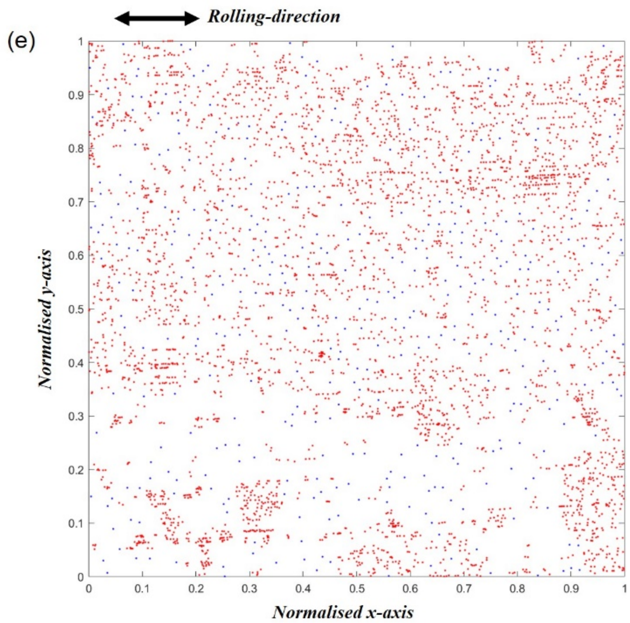

Figure 8. Reconstructed, centroid spatial-distribution of (a) inclusions in S45-0, (b) pits in S45-0.5, (c) pits in S45-2.0, (d) pits in S45-4.0 and (e) pits in S45-6.0, after inclusions and pits had been classified into two groups: red = cluster-sets and blue = random background-sets.

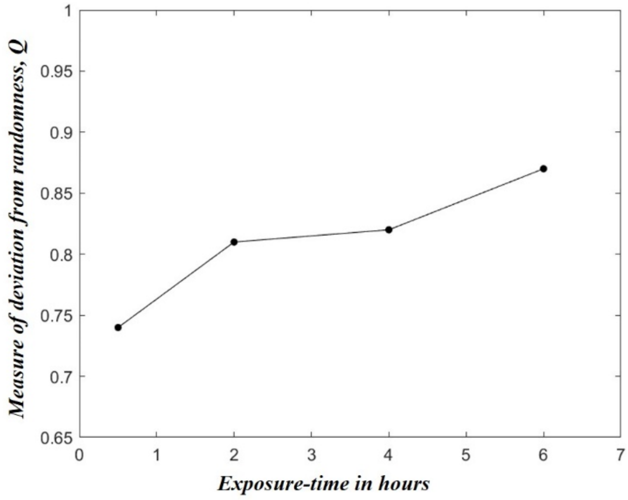

Figure 9. The *Q* value for pit-distribution in JIS-S45C, as a function of exposure-time.

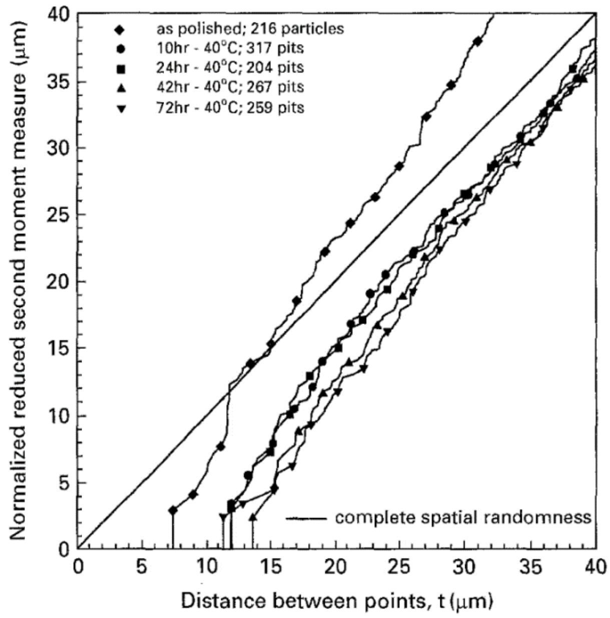

Figure 10. Estimation of *K* for 2024-T3 aluminum alloy-specimens, before and after exposure to a 0.5M-NaCl solution for 10, 24, 42 and 72 hours at 40°C [21].

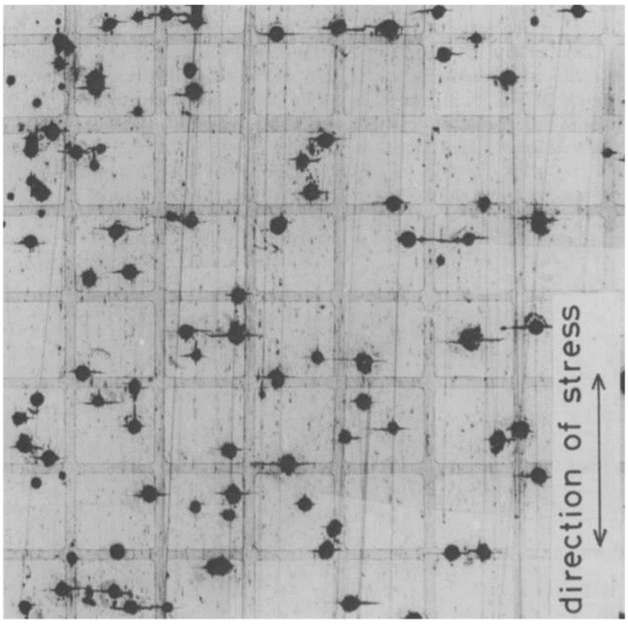

Figure 11. Multiple corrosion-fatigue cracks on the surface of a high-strength-steel plate, after exposure to a corrosive environment at a stress-range of 235 MPa after one million cycles. All the cracks initiated from corrosion-pits [10].

Tables

Table 1. Chemical composition of a medium-carbon steel, JIS-S45C, in wt.%.

C	Si	Mn	P	S
0.47	0.21	0.82	0.018	0.018

Table 2. Mechanical properties of a medium-carbon steel, JIS-S45C.

Elongation, %	Reduction in area, %	0.2% proof-stress, MPa	Tensile-strength, MPa
18.5	53.8	339	620

Table 3. Identification of specimens and their corresponding exposure-times.

Specimen	S45-0	S45-0.5	S45-2.0	S45-4.0	S45-6.0
Exposure-time (hours)	0	0.5	2.0	4.0	6.0

Table 4. Main results of the statistical analysis of pit-data, using the QR method.

Exposure-time, in hours	0	0.5	2.0	4.0	6.0
Size of area, in $\mathbf{unit^2}$	1	1	1	1	1
$\boldsymbol{N}$	3935	3773	3253	2735	4219
$\boldsymbol{\rho}$	3935	3773	3253	2735	4219
$\boldsymbol{\bar{r}_1}$	0.0061	0.006	0.0071	0.0078	0.0067
$\boldsymbol{E(\bar{r}_1)}$	0.008	0.0081	0.0088	0.0096	0.0077
$\boldsymbol{Q}$	0.77	0.74	0.81	0.82	0.87
$\boldsymbol{s_1}^{\mathbf{2}}$	3.73×10^{-5}	3.81×10^{-5}	4.89×10^{-5}	5.41×10^{-5}	3.12×10^{-5}
$\boldsymbol{E(s_1{}^2)}$	1.74×10^{-5}	1.81×10^{-5}	2.09×10^{-5}	2.49×10^{-5}	1.62×10^{-5}
$\boldsymbol{R}$	2.15	2.10	2.33	2.17	1.92
$\boldsymbol{\sigma_{E(\bar{r}_1)}}$	6.64×10^{-5}	6.93×10^{-5}	0.80×10^{-5}	9.56×10^{-5}	6.19×10^{-5}
$\boldsymbol{c}$	28.6	30.3	21.6	18.84	16.14
Probability of a greater difference between $\boldsymbol{\bar{r}_1}$ **and** $\boldsymbol{E(\bar{r}_1)}$	$< 1.0 \times 10^{-7}$	$< 1.0 \times 10^{-7}$	$< 1.0 \times 10^{-7}$	$< 1.0 \times 10^{-7}$	$< 1.0 \times 10^{-7}$